Fabrication of 3D Core–Shell Multiwalled Carbon Nanotube@RuO_2 Lithium-Ion Battery Electrodes through a RuO_2 Atomic Layer Deposition Process

Keith E. Gregorczyk,[†,‡] Alexander C. Kozen,[†,‡] Xinyi Chen,[†,‡] Marshall A. Schroeder,[†,‡] Malachi Noked,[‡] Anyuan Cao,[§] Liangbing Hu,[†] and Gary W. Rubloff*[,†,‡]

[†]Department of Materials Science and Engineering, University of Maryland, College Park, Maryland 20742, United States, [‡]Institute for Systems Research, University of Maryland, College Park, Maryland 20742, United States, and [§]Department of Materials Science and Engineering, College of Engineering, Peking University, Beijing 100871, People's Republic of China

ABSTRACT Pushing lithium-ion battery (LIB) technology forward to its fundamental scaling limits requires the ability to create designer heterostructured materials and architectures. Atomic layer deposition (ALD) has recently been applied to advanced nanostructured energy storage devices due to the wide range of available materials, angstrom thickness control, and extreme conformality over high aspect ratio nanostructures. A class of materials referred to as conversion electrodes has recently been proposed as high capacity electrodes. RuO_2 is considered an ideal conversion material due to its high combined electronic and ionic conductivity and high gravimetric capacity, and as such is an excellent material to explore the behavior of conversion electrodes at nanoscale thicknesses. We report here a fully characterized atomic layer deposition process for RuO_2, electrochemical cycling data for ALD RuO_2, and the application of the RuO_2 to a composite carbon nanotube electrode scaffold with nucleation-controlled RuO_2 growth. A growth rate of 0.4 Å/cycle is found between ~210–240 °C. In a planar configuration, the resulting RuO_2 films show high first cycle electrochemical capacities of ~1400 mAh/g, but the capacity rapidly degrades with charge/discharge cycling. We also fabricated core/shell MWCNT/RuO_2 heterostructured 3D electrodes, which show a 50× increase in the areal capacity over their planar counterparts, with an areal lithium capacity of 1.6 mAh/cm^2.

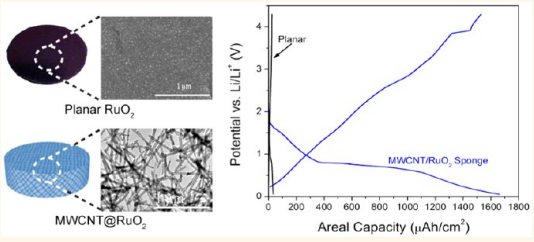

KEYWORDS: atomic layer deposition · ruthenium oxide · conversion electrode · Li-ion battery · multiwalled carbon nanotubes

One of the most promising routes to increasing both gravimetric and areal energy density of Li-ion batteries has emerged through the development of heteronanostructured devices. Such devices, because of a drastic increase in surface area and decrease in thickness of the electrochemically active materials, demonstrate power densities orders of magnitude above their planar counterparts.[1−5] Atomic layer deposition (ALD), with its angstrom-level thickness control, ability to coat high aspect ratio structures, and wide availability of materials, is ideally suited to fabrication of these heteronanostructures.[6−15]

A few reports exploiting ALD's extreme conformality have shown dramatic increases in areal capacity when active materials are deposited on, or into, high surface area substrates, such as nanowires, nanorods, and/or nanopores. For anodes, the relatively low capacity material TiO_2 (150 mAh/g) has been deposited on Al nanorods, Ni nanowires, and biotemplated tobacco mosaic virus (TMV) substrates.[16−19] ALD processes have also been developed for higher capacity materials such as Co_3O_4 (374 mAh/g) for cathodes and SnO_2 (782 mAh/g) for anodes.[20,21] Finally, our group has developed a new process capable of depositing crystalline V_2O_5, a cathode material with a

* Address correspondence to rubloff@umd.edu.

Received for review October 3, 2014 and accepted December 17, 2014.

Published online December 17, 2014
10.1021/nn505644q

relatively high theoretical capacity (294 mAh/g, forming $Li_2V_2O_5$)[22] and applied it to make high surface area electrodes using TMV and multiwall carbon nanotube (MWCNT) sponges.[23−25] More recently, we have demonstrated fabrication of a full Li-ion battery array based on these concepts patterned on an anodic aluminum oxide template.[26]

RuO_2 is attractive for lithium ion batteries (LIBs) due to its high, metal-like, electronic conductivity (36.2 $\mu\Omega$-cm resistivity) and high theoretical capacity for the conversion reaction down to 0.9 V *vs* Li/Li^+ (806 mAh/g).[27] Its experimentally measured capacity, when discharging to lower potentials, has been reported to be as high as 1310 mAh/g due to more complicated mechanism of Li storage below the potential for conversion reaction, and formation of new phases of Ru/Li_2O and solid electrolyte interface (SEI).[28,29] Those studies pointed out RuO_2 as a system well suited for understanding the complicated heterogeneous reaction of Li storage and pave the way for promising application of high capacity conversion electrodes. Despite this promise and considering the advantages ALD offers concerning the fabrication of high-aspect ration heteronanostructures (as discussed in the previous paragraph), very little work has been done to develop an ALD process for RuO_2, and no electrochemical study of ALD RuO_2 has been reported.

A number of precursors have been developed to deposit Ru metal through ALD,[30] typically using a Ru-containing metal−organic and O_2 as the precursors. Several of these process investigations have noted that if the O_2 partial pressure was increased during the reaction RuO_2, rather than Ru, could be deposited. Using bis(cyclopentadienyl)ruthenium ($RuCp_2$), a significant increase in the growth rate per cycle (GPC) from 1.2 to 3.2 Å/cycle was seen as a function of increased oxygen partial pressure and was accompanied by an increase in film resistivity.[31] Much more prevalent has been the use of bis-(ethycyclopentadienyl)ruthenium ($Ru(EtCp)_2$) where several reports have noted an increase in the GPC and resistivity of the resulting ALD films measured through a variety of standard techniques (4-pt probe, Hall, *etc.*). Characterization through X-ray diffraction (XRD) and X-ray photoelectron spectroscopy (XPS) showed that these films were RuO_2, with reported growth rates varying between 1.4 and 1.6 Å/cycle.[31−35] A modified ALD process, in which a constant partial pressure of O_2 was held during the reaction, also used $Ru(EtCp)_2$ and resulted in RuO_2 films.[36] An in situ IR-spectroscopy study reported the formation of RuO_2 using cyclopentadienyl ethylruthenium dicarbonyl ($Ru(Cp)(CO)_2(Et)$) after a nucleation period of 1−5 cycles where only Ru particles were observed.[37] This study reported a GPC range between 1.5 and 3 Å/cycle, but only studied out to 25 ALD cycles. A liquid injection ALD process using bis(2,2,6,6-tetramethyl-3,5-heptanedionato)(1,5-cyclooctadiene)ruthenium, $Ru(thd)_2(COD)$, dissolved in iso-octane, reported a GPC of 6.6 Å/cycle for processes between 20 and 60 cycles.[38] Another report used $Ru(od)_3$/*n*-butyl acetate solution to deposit Ru onto carbon nanotubes (CNT), which were then annealed at 500 °C in O_2, which oxidized the film and removed the CNT template.[39] Finally, our previous results using bis(2,6,6-trimethyl-cyclohexadienyl)ruthenium also noted that if the partial pressure of O_2 was increased a phase change was seen in the XRD spectra.[30] We emphasize that despite these numerous observations of RuO_2 growth during Ru-based processes no fully optimized parameters (*i.e.*, precursor and oxidant dosage saturation curves, temperature window, and resulting film properties) have been published.

As a LIB material, RuO_2 is in a class of materials called the conversion electrodes, incorporating Li through the reversible chemical reaction: $RuO_2 + 4e^- + 4Li^+ \leftrightarrow Ru^0 + 2Li_2O$.[27,40] Conversion electrodes represent a broad class of materials that includes oxides, sulfides, nitrides, fluorides, and phosphides.[27] In bulk form RuO_2 has been studied using commercial powder, carbon black, graphite, and polyvinylene diflouride mixed in a 10:1:1:1 ratio which showed a capacity of 1130 mAh/g; however, the battery was only able to be cycled three times before failure occurred.[28] The same group showed an enhanced capacity in amorphous RuO_2 and the possibility of interfacial charge storage.[29,41−43] *In situ* transmission electron microscopy (TEM) detailed the chemical and mechanical changes during lithiation, including the identification of the intermediate Li_xRuO_2 witnessed using *ex situ* TEM measurements of cycled electrodes.[44,45]

In this paper we report the first fully developed RuO_2 ALD process and show optimized process parameters. We studied the performance of planar films as conversion electrode materials for direct comparison to other bulk systems studied in the literature, showing the first galvanostatic cycling data for RuO_2. Taking advantage of ALD's unparalleled ability to coat high-aspect ratio nanostructures, multiwalled carbon nanotube (MWCNT) sponges were employed as highly conductive, high aspect ratio substrates. MWCNT sponges (~2 mm thick) were conformally coated using the process parameters developed here; these heterostructured electrodes showed dramatically higher areal capacities (×50) and improved cyclability over their planar counterparts. The results reported here also represent the first study of self-standing RuO_2 electrodes for electrochemical energy storage without use of binders, and other additives required when fabricating powdered material electrodes.

RESULTS AND DISCUSSION

ALD Process Optimization. In order to observe the self-limited chemisorption reaction characteristic of an ALD

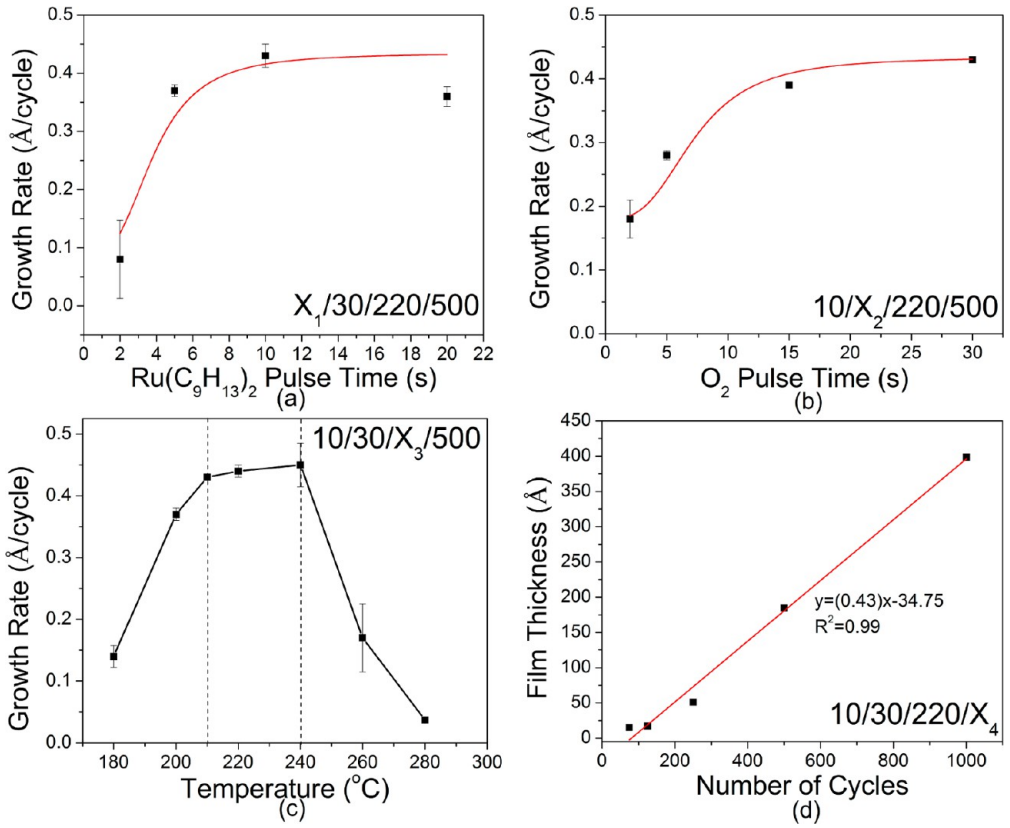

Figure 1. ALD process parameters, $Ru(C_9H_{13})_2$ pulse time/O_2 pulse time/temperature/number of cycles denoted as $X_1/X_2/X_3/X_4$ in each figure. (a,b) Saturation curves for $Ru(C_9H_{13})_2$ and O_2, respectively, each showing a saturated growth rate of ~0.4 Å/cycle. (c) The temperature window using the optimized process parameters. (d) Film thickness *versus* number of cycles confirming the saturated growth rate of 0.43 Å/cycle observed in (a) and (b) and also showing a nucleation period of 70−80 cycles.

process, the growth per cycle (GPC) was monitored as a function of $Ru(C_9H_{13})_2$ dose, O_2 dose, and substrate temperature. The results for these experiments are shown in Figure 1(a−c). First we consider the $Ru(C_9H_{13})_2$ dose. While holding the O_2 pulse time at 30 s, the $Ru(C_9H_{13})_2$ pulse was varied from 2 to 20 s the results of which are shown in Figure 1(a). Saturated ALD growth rates are seen for pulses 5 s and longer giving a growth rate of 0.4 Å/cycle. Next the $Ru(C_9H_{13})_2$ pulse was held constant at 10 s, well within the saturated regime, and the O_2 pulse time was varied between 4−30 s with the results shown in Figure 1(b). Once again a saturated GPC of 0.4 Å/cycle is seen, for pulse times 15 s and longer.

Figure 1(c) shows the temperature window for the $Ru(C_9H_{13})_2$−O_2 ALD RuO_2 process as a function of substrate temperature from 180 to 280 °C under the above optimized exposure and purge conditions (*i.e.*, 10 s $Ru(C_9H_{13})_2$, 30 s O_2, and 5 s Ar purge). These data show a clear temperature window between 210 and 240 °C where the GPC remains constant at 0.4 Å/cycle. The sharp drops in the GPC observed for temperatures below 210 °C and above 240 °C are common characteristics of ALD processes, where there is an incomplete reaction at lower temperatures (here, below 210 °C) and where thermal desorption of the molecule and/or a loss of surface species occur at higher temperatures (here, above 240 °C).[46]

To understand the nucleation kinetics of this RuO_2 ALD reaction, the film thickness was measured as a function of cycle number using the optimized process parameters. The substrate temperature was held at 220 °C, well within the temperature window, and films were deposited at 75, 125, 250, 500, and 1000 cycles, the results are shown in Figure 1(d). A linear fit is obtained, with two important consequences. First, the slope of the fit gives a GPC of 0.43 Å/cycle, consistent with the rest of the process parameters shown in Figure 1(a−c) and second, by extrapolating the fit through the *x*-axis the nucleation period can be estimated as ~70−80 cycles.

Characterization of RuO_2 Films. To determine the crystal structure, thick films (1000 cycles, ~40 nm) were deposited on SiO_2 and XRD patterns were obtained with the results shown in Figure 2. From these data it is clear that these films are poly crystalline and nanograined. The dominant peaks are the overlapping RuO_2(110) and RuO_2(101), however smaller peaks are visible for the RuO_2(011), RuO_2(211), RuO_2(002), and RuO_2(112) reflections. The dominant film orientation is either the (101) or (011) direction (lattice parameters a = 4.492 Å and c = 3.107 Å). Given this and the GPC,

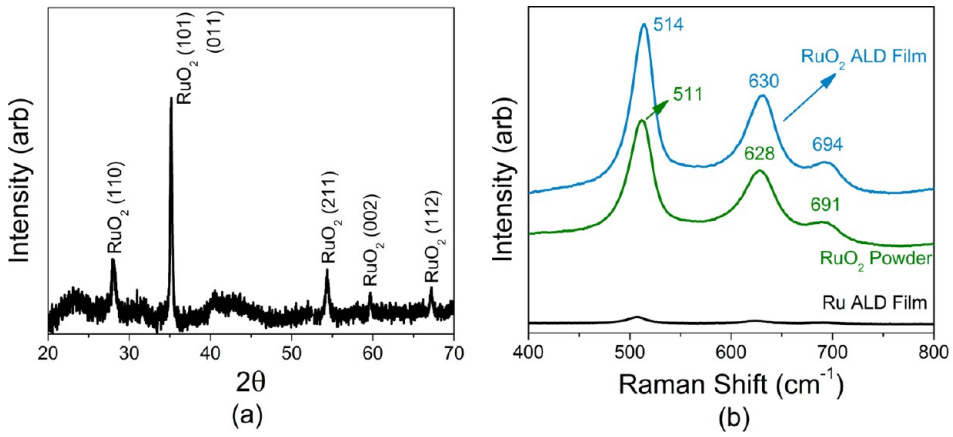

Figure 2. Characterization of the RuO_2 ALD films. XRD (a) shows that the films are polycrystalline with a dominate peak corresponding to the RuO_2 (101) and RuO_2 (011) reflections. Raman spectroscopy (b) was done to compare the local structure of the films to that of purchased powder and shows a 1:1 overlap. Ru ALD films only show small peaks due to native oxide growth, but otherwise confirm the uniqueness of the two processes.

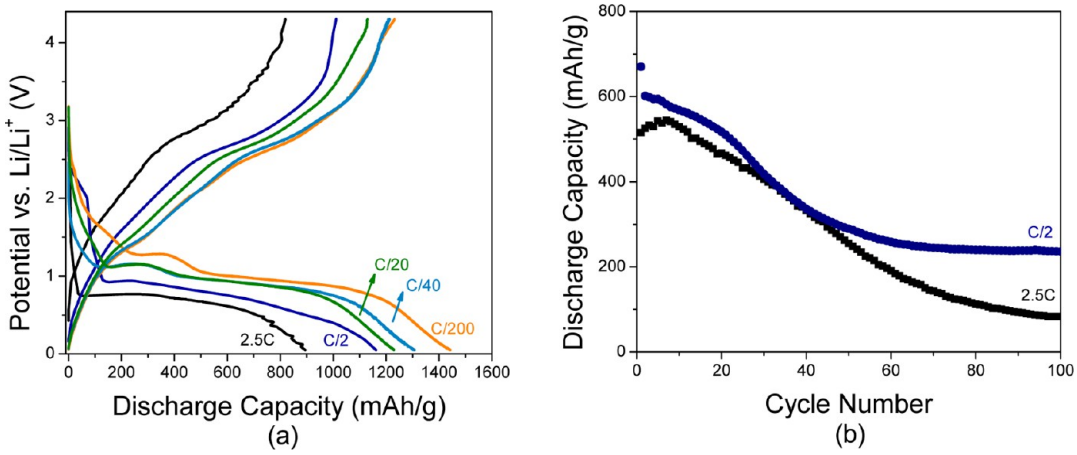

Figure 3. Electrochemical characterization of RuO_2 ALD fabricated into a standard coin cells. First cycle discharge capacities (a) showing a high capacity 1450 mAh/g at C/200, 1300 mAh/g at C/20, 1200 mAh/g, 1100 mAh/g at C/2, and 900 mAh/g at 2.5C. Plateaus corresponding to $Li_{0.86}RuO_2$, seen at ~1.25 V for C/200 and ~1.1 V at C/40 and C/20, $Li_{1.2}RuO_2$ at ~1 V, and a matrix of Ru/Li_2O at 0.05 V. The cyclability of these electrodes is shown in (b) for C/2 and 2.5C. The capacity is seen to drop to ~400 mAh/g after 40 cycles for C/2. At 2.5C the capacity is seen to increase for the first 10 cycles and then falls to ~150 mAh/g.

we calculate that only ~0.1 monolayer (ML) of RuO_2 is deposited per cycle, well below the nominal 1 ML/cycle expected of a prototypical ALD process. However, similar results have been reported for the well-studied $RuCp_2$ system for Ru ALD, where a 0.2 ML/cycle growth rate was observed.[31,47]

Further structural information was gathered through Raman spectroscopy. Thick films (1000 cycles, ~40 nm) were deposited on SiO_2 substrates and were compared to a commercially purchased RuO_2 powder (Sigma-Aldrich), as well as metallic ALD Ru films deposited with the same precursor using our previously published ALD process, the results of which are shown in Figure 2(b).[30] The spectrum for crystalline RuO_2 has three modes, E_g at 528 cm^{-1}, A_{1g} at 644 cm^{-1}, and B_{2g} at 716 cm^{-1}.[48] All three modes are visible in our results. In comparison to the purchased powder a nearly 1:1 overlap between the RuO_2 powder peaks and the ALD RuO_2 films peaks can be seen. Only small versions of the RuO_2 peaks, due to native oxide growth, are seen on the ALD Ru films.

Electrochemical Studies. *Planar.* After deposition the mass of ~80 nm films (2000 cycles) was measured to be ~150 μg, and the samples were cycled between 4.3 and 0.05 V *vs* Li/Li^+. The first cycle discharge/charge curves for different C rates are shown in Figure 3(a). The highest capacity is seen for the discharge rate of C/200, namely ~1450 mAh/g, comparable to measured capacities mentioned in the literature at this potential window.[28,29] The expected lithiation reaction is $RuO_2 + 4e^- + 4Li^+ \leftrightarrow Ru^0 + 2Li_2O$, which produces two species in the fully discharged state, Ru and Li_2O. Experiments with micron sized RuO_2 powders have confirmed that after full discharge the Ru becomes nanosized particles in a Li_2O matrix.[28] Other work has shown that extra Li^+ can be stored at the Ru/Li_2O interface.[43] We therefore attribute the excess capacity measured at this slow discharge rate to the formation

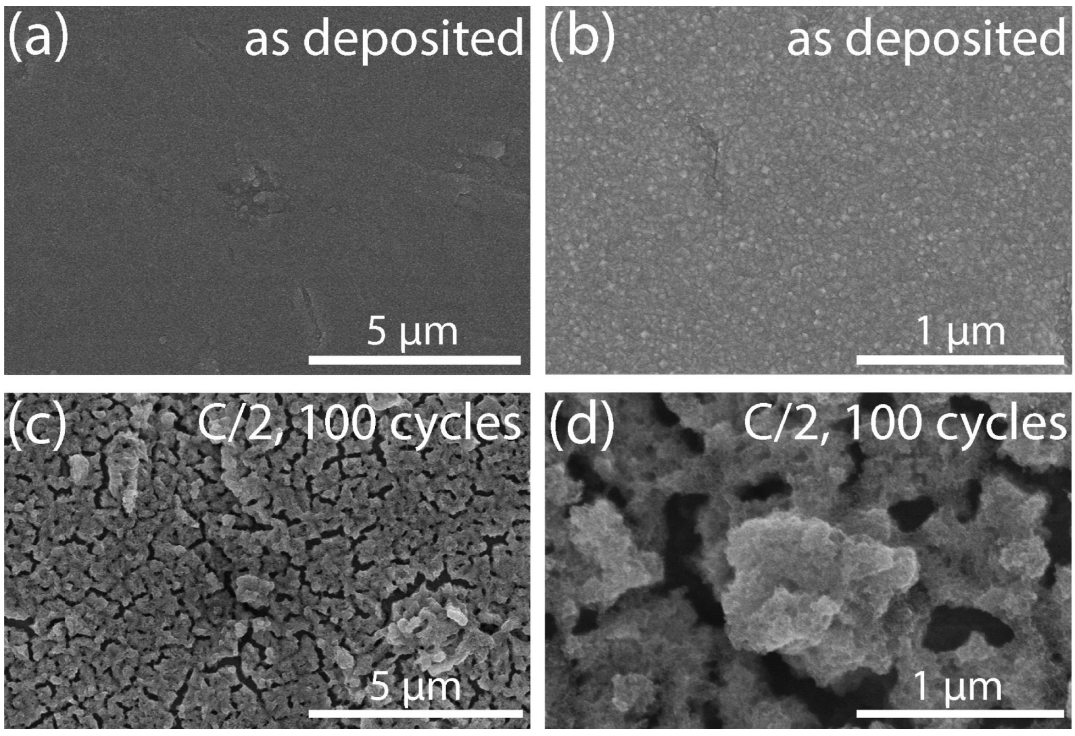

Figure 4. SEM images of RuO_2 ALD films deposited on stainless steal discs before and after cycling. (a,b) High and low magnification images of the as deposited films. (c,d) The same two scales after the batteries were cycled 100 times at C/2. These images show significant morphological changes and degradation after cycling.

of heterogeneous Li phases on the electrode interface, as suggested by other conversion electrode systems.

As expected, faster C rate discharges show a decline in gravimetric capacity. At C/40 the capacity is 1300 mAh/g, decreasing to 1200 mAh/g at C/20. All three of these curves (C/200, C/40, C/20) show similar structure with two plateaus visible. The first small plateau is seen at 1.25 V for C/200 and appears at 1.1 V for the C/40 and C/20 rates. According to the previously published RuO_2 bulk data this first plateau corresponds to $Li_{0.86}RuO_2$.[29] The second and larger plateau visible at ~1 V for C/200, C/40, and C/20 corresponds to $Li_{1.2}RuO_2$ according to the same reference. Finally the tail of the curves, which dips down to 0.05 V, correspond to the fully lithiated phase where the reaction has gone to completion and, as mentioned, has been shown to be a network of Ru nanoparticles in a Li_2O matrix.[44] Generally these curves compare well to those reported in the literature, though an exact comparison is not possible since no pure RuO_2 results have been reported.[28,29]

At the fastest two rates studied, C/2 and 2.5C, the capacity of the films decreases and the discharge curve's shape also changes. At C/2, the films show a capacity of over 1100 mAh/g, while the 2.5C the capacity decreases to 900 mAh/g. The plateaus corresponding to the $Li_{0.86}RuO_2$ phase are no longer visible and the large plateau for the $Li_{1.2}RuO_2$ phase gradually slopes into the tail corresponding to the Ru/Li_2O mixture. At high lithiation rates insertion of lithium into the amorphous interstitial phase is favorable over crystalline Li_2O formation due to faster reaction kinetics. These results compare well to *in situ* TEM measurements of RuO_2 nanowires that showed a 95% volume expansion during lithiation, 26% of which is irreversible due to a loss of both ionic and electronic conductivity, and where the Li_xRuO_2 phase was only seen at very slow scan rates.[44]

Figure 3(b) shows the cyclability of the ALD RuO_2 films at C/2 and 2.5C. The C/2 data shows a quick decrease in capacity from 1200 to 1000 mAh/g after the first cycle. After the first two cycles, the capacity steadily declines and stabilizes at ~400 mAh/g after 60 cycles. The 2.5C data shows an increase in capacity for the first 10 cycles after which it steadily declines, never fully saturating but dropping to a capacity of ~150 mAh/g after 100 cycles. It may be that for the higher rate (2.5C) in the first few cycles not all of the mass of ALD RuO_2 is used, and that as the battery is cycled more of the material is utilized, resulting in an apparent increase in capacity. After this initial increase the capacity decays similar to the C/2 battery. No cyclability data are available in the literature for comparison.

The capacity degradation can be partially understood through the dramatic structural changes seen in the SEM images in Figure 4 (a–d). The as-deposited films are shown in Figure 4(a,b) and show smooth and nanograined films, only showing scratches from the stainless steel disc substrate. After cycling at C/2 for

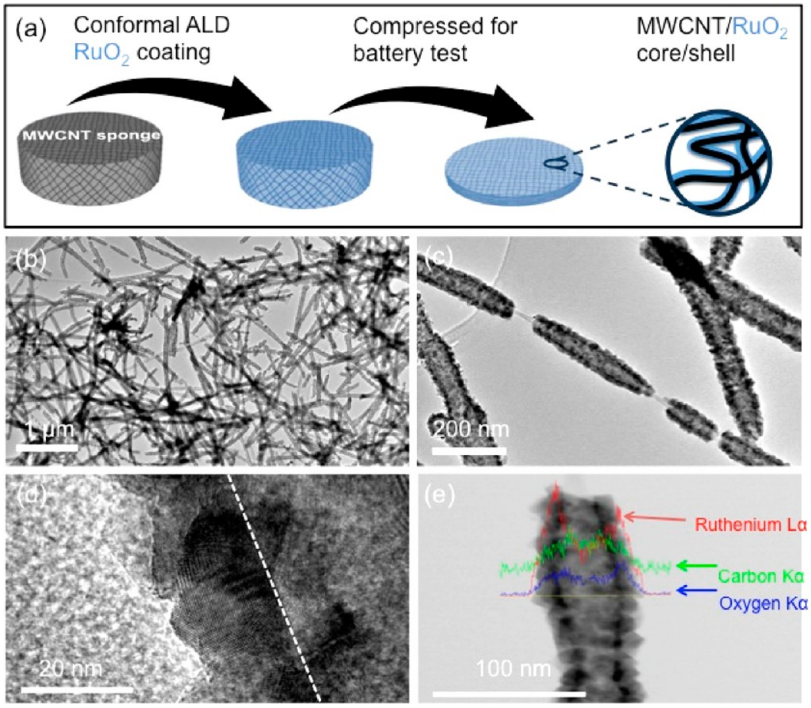

Figure 5. Fabrication of MWCNT/RuO_2 heterostructured electrodes. (a) A schematic of the process where the MWNCT sponge is cut into desired dimensions, coated with 600 cycle of RuO_2 (~20 nm), and then compressed into a coin cell battery for testing. TEM results (b−e) confirm that the coating is conformal over high surface area of the MWCNT sponge. The high-resolution image in (d) confirms the thickness of the film and that it is polycrystalline, the dotted line denotes the edge of the MWCNT. Scanning EDS (e) further confirms the core/shell nature with Ru and O peaks strongest on the edges and C in the middle. (a) was adapted from ref 25.

100 cycles the films were imaged again at the same magnifications as seen in Figure 4(c,d). These results are again consistent with *in situ* TEM measurements that show a strong correlation between mechanical degradation and loss of capacity due to chemical irreversibility.[44]

3D MWCNT@RuO_2 Electrodes. To take advantage of ALD's extreme conformality 3D MWCNT/RuO_2 heterostructured electrodes were fabricated. This incredibly high aspect ratio substrate allowed a large mass of material to be deposited as a thin film in a small area dramatically increasing the areal capacity. A diagram of the MWCNT/RuO_2 core/shell fabrication process can be seen in Figure 5(a). After the growth of the MWCNT sponge they were cut into the desired size (1/8 in. diameter, 2 mm thick) and coated with 600 cycles of ALD RuO_2 along with the stainless steel discs that were used as controls. TEM images of the MWCNT/RuO_2 core/shell nanowires are shown in Figure 5 (b−e). The random dispersion shown in Figure 5(b) confirms that the coating is conformal over the large area (*i.e.*, entire 2 mm). Closer inspection, Figure 5(c), shows a conformal coating of ~20 nm slightly below (0.33 Å/cycle) the GPC discussed previously, as well as a few uncoated areas, because of this slight difference the planar samples will have a thickness of ~24 nm, slightly thicker. Growth on MWCNTs has been consistently shown to require defect sites, hydroxyl groups, or carboxyl groups to begin nucleation, the film then grows from that cite coating the tube.[49−51] Figure 5(d) shows a high-resolution image of the coating where polycrystalline grains can be seen, consistent with the XRD and SEM results in Figure 2 and 4 respectively. The core/shell structure is further confirmed in Figure 5(e) using line scan EDX showing Ru and O 1s peaks strongest on the edges and C 1s peaks strongest in the center. The crystallinity and oxidation state of the RuO_2 was further confirmed with XRD and XPS, the data of which can be found in the Supporting Information Figures S1 and S2.

Similar to the planar study discussed above the MWCNT sponge was weighed before and after deposition with an average weight increase of ~500 μg over the 1/8 in diameter electrode area (corresponding to >6 mg/cm^2). A ~17× increase in mass loading was seen, whereas planar control samples placed in the ALD reactor simultaneously only showed ~30 μg increase. To test the electrochemical properties of the MWCNT/RuO_2 core/shell electrodes they were fabricated into standard coin cells as discussed in the Experimental Details section and were also cycled between 4.3 and 0.05 V against Li/Li$^+$ for comparison to the planar results discussed above. The results of these experiments are shown in Figure 6.

The results for the first cycle areal discharge are shown in Figure 6(a). The MWCNT/RuO_2 nanowires show a ~50× increase in capacity over the planar control

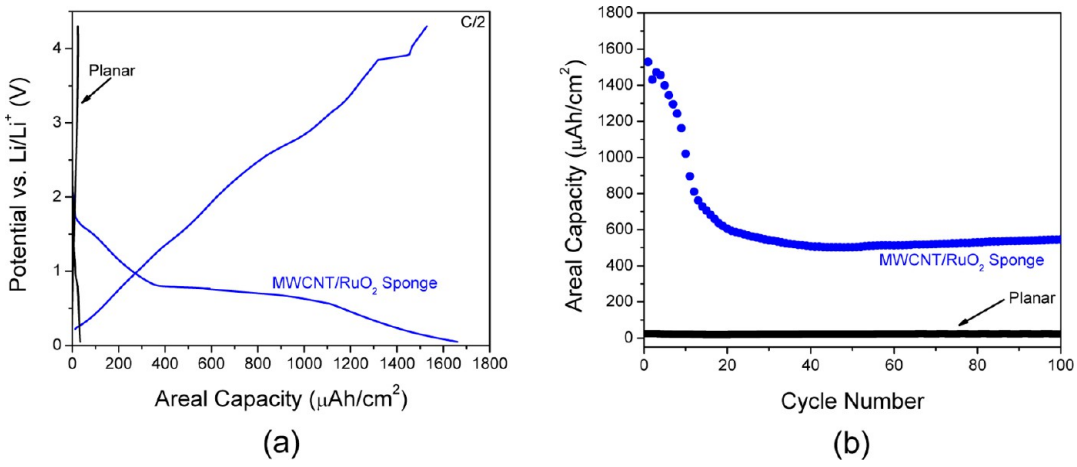

Figure 6. Electrochemical evaluation of the MWCNT/RuO_2 sponge electrodes. The first cycle areal capacity for the control planar sample (600 cycles on a stainless steel disc) and the MWCNT/RuO_2 electrode (600 cycles on MWCNT sponge) is shown in (a). A ~50× increase in the areal capacity is seen where the planar control sample capacity was ~30 μAh/cm^2 increasing to ~1600 μAh/cm^2 for the MWCNT/RuO_2. The areal cycle stability is shown in (b) where the initial high capacity of the MWCNT/RuO_2 drops to ~600 μAh/cm^2 after the first 20 cycles and then remains stable. The planar sample also decreases from ~30 to ~20 μAh/cm^2.

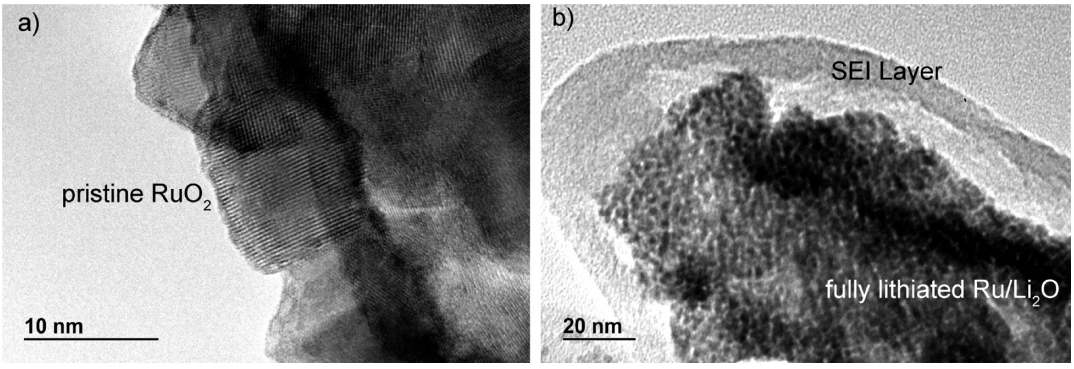

Figure 7. Transmission electron microscopy images of the as-deposited ALD RuO_2 on the MWCNT sponge (a), and the fully lithiated structure showing the nanostructured network of Ru and Li_2O (b). The crystallinity of the RuO_2 is easily visible after deposition on the MWCNT sponge. After lithiation two important details become apparent. First is the formation of the SEI layer, which has been discussed extensively in the literature.[28,43,53] Second is the formation of the nanostructured network of Ru and Li_2O, which has also been shown previously.

samples with values of ~1.6 *vs* ~0.03 mAh/cm^2 respectively. The cycle stability was also tested, with the results displayed in Figure 6(b). Despite the high initial capacity for the MWCNT/RuO_2 nanowires the capacity decreases to ~0.6 mAh/cm^2 after 20 cycles. The planar control sample also shows a decrease in capacity that is not visible due to the scale of the figure, but decreases to a value of ~0.02 mAh/cm^2. Changes in the structure of the MWCNT/RuO_2 can be seen in the TEM images in Figure 7, where the initially crystalline RuO_2 becomes a nanostructured network of Ru and Li_2O. The results shown here confirm the reaction scheme discussed in the introduction to the paragraph and compares completely to previously published work.[28,43,44] Furthermore, the formation of the secondary electrolyte interphase (SEI) can be seen, also contributing to some loss of capacity.

Despite the formation of the SEI, these results indicate that the 3D core/shell heterostructure allows the ALD RuO_2 to retain a higher capacity over the planar control for two reasons. First, the large surface area of the MWCNT sponge allows a large mass of RuO_2 to be deposited in very thin films. The thin film allows faster electronic and ionic conduction and helps to prevent the mechanical degradation seen in the SEM images for thicker films (Figure 4). Furthermore, the high conductivity MWCNTs act as facile pathway for electrons to access the active material. Additionally, the heterogeneous structure of the MWCT\RuO_2 electrode, enabled better cycling performances previously reported in literature for RuO_2 conversion electrode, suggesting that electrode with complicated Li storage mechanism can demonstrate better stability in well controlled heterogeneous architecture.

CONCLUSIONS

The high initial capacity of RuO_2, expected from its theoretical capacity, makes it attractive for lithium ion

storage, though this promise is significantly compromised by its capacity degradation as seen at higher rates or due to cycling. The prominent structural changes observed by SEM and TEM suggest degradation mechanisms linked to structural change, one of the many fundamental mechanisms that control capacity degradation, all of which remain a pervasive challenge in electrochemical storage across a wide range of materials. Despite this degradation the ability to synthesize high capacity RuO_2 by ALD is promising in two senses. First, ALD is uniquely capable of the high conformality and deposition control needed for fabrication of heterogeneous nanostructures, *e.g.*, incorporating current collector, active storage material, and passivation (or artificial SEI) layers. By making such structures, as shown with the MWCNT/RuO_2 core/shell electrodes, it is possible to subvert some of these mechanism and several groups and a significant amount of literature using ALD, as mentioned in the introduction, has begun address this question. Second, such heterogeneous nanostructures open new possibilities for robust electrode designs (*e.g.*, nanowires) less susceptible to degradation at high rates and upon cycling.[52] Together these factors argue in favor of applying ALD RuO_2 (and other ALD materials) to nanostructured electrodes to better understand degradation mechanisms and to achieve significantly better capacity retention.

Furthermore, the ALD process developed here in combination with the extreme conformality shown by depositing on the MWCNT sponges may have considerable applications in other fields. This high conformality may have significant applications in the semiconductor industry, which seeks to use RuO_2 as an electrode in trench capacitors. The crystallinity of the film may also present unique opportunities in catalysis. During the nucleation period of growth, individual islands of crystalline RuO_2 may be present offering the possibility of making new catalysis materials.

EXPERIMENTAL DETAILS

A custom built cross-flow reactor with a base pressure of 10 mTorr was used to develop the RuO_2 ALD process. The metal–organic Ru precursor, bis(2,6,6-trimethyl-cyclohexadienyl)-ruthenium, $Ru(C_9H_{13})_2$ (or "Cyprus", Air Liquide), was loaded into a Strem electropolished stainless-steel bubbler and maintained at 80 °C. Ar (99.99%, Praxair) was flowed through the bubbler at 100 sccm. Research grade O_2 (99.999%, Praxair) was used as the oxidant and was flowed at 400 sccm. Timed Swagelok ALD valves controlled the dose for both precursors. One optimized ALD cycle consisted of the following pulse/purge sequence: 10 s $Ru(C_9H_{13})_2$ pulse, 5 s Ar purge, 30 s O_2 pulse, 5 s Ar purge. Process optimization was done on 50 mm Si wafers.

Material characterization was done using a Horiba Jobin-Yvon LabRAM HR-VIS MicroRaman system with a 632.8 nm laser source. To determine the crystallinity of the films, X-ray diffraction (XRD) was done with a Bruker D8 Advance system with LynxEye PSD detector and Ni β-filter using Cu Kα (1.54 Å) radiation. Samples prepared for Raman spectroscopy and XRD were deposited on 1 cm $\times$ 1 cm glass slides cleaned in an acidic piranha solution for 5 min, rinsed with deionized water (DIW), and blown dry with N_2 before deposition.

Film thicknesses were measured *ex situ* with a Sopra GES5 spectroscopic ellipsometer. Thickness profiles for each wafer, unless otherwise noted, were mapped by measuring 5 points along the gas flow direction. The average thickness of these points is reported as the thickness and the nonuniformity was estimated from the ratio of the standard deviation of the 5 points divided by the mean. Scanning electron microscopy (SEM) and transmission electron microscopy (TEM) images were obtained with a Hitachi SU-70 and JEOL 2100 FE-TEM/STEM respectively.

For electrochemical testing coin-type half-cells *versus* Li/Li^+ were fabricated. Stainless-steel discs were degreased by sonication in a 1:1 mixture of isopropyl alcohol and acetone for 10 min and blown dry with N_2. They were then weighed before and after deposition using a Mettler Toledo XS105 dualRange microbalance with a resolution of 1 μg. For the planar studies $\sim$150 μg (2000 cycles) of RuO_2 was deposited using the optimized parameters. For the 3D MWCNT/RuO_2 studies CNT sponges and stainless steal discs were loaded into the reactor at the same time, with the discs serving as control samples. 600 cycles, $\sim$20 nm on the MWCNT and $\sim$24 nm on the stainless steel dics, of RuO_2 was deposited which correspond to mass increases of $\sim$500 μg for the MWCNT sponges and $\sim$30 μg for the planar control samples. All samples were dehydrated overnight at 100 °C before cell assembly. CR 2032 Coin cells (MTI) were fabricated in a dry Ar filled glovebox with lithium metal (Sigma-Aldrich) as the counter electrode, a Celgard separator (Celgard 3501), and 1 M $LiPF_6$ in a 1:1 mixture of ethylene carbonate (EC) and diethyl carbonate (DEC) (Novolyte Technologies) as the electrolyte. An Arbin BT-2000 multichannel battery test station was used for galvanostatic, rate capability, and life cycle testing.

Multiwalled carbon nanotube (MWCNT) sponges were grown by chemical vapor deposition (CVD) using 1,2-dicyclobenzene as the carbon source and ferrocene as the catalyst. Ferrocene powder was dissolved into 1,2-dicyclobenzene to make a solution with a concentration of 0.06 g/mL. The solution was then injected into a 2 in. quartz tube CVD furnace by a syringe pump at a constant feeding rate of 0.13 mL/min. The carrier gas was a mixture of Ar and H_2, at a flow rate of 2000 and 300 mL/min, respectively. Quartz slides were used as the growth substrates that were placed in the center of the furnace at 860 °C. Typically the growth time was 4 h, which gives bulk sponge samples with thicknesses of about 8–10 mm. Before ALD coating the samples were cut into 1/8 in. diameter, 2 mm thick samples. Further information on this process can be found in the following references.[25,53,54] Battery testing with the coated MWCNT sponges were also done in CR2032 coin cells as described above.

Conflict of Interest: The authors declare no competing financial interest.

Acknowledgment. This work has been supported by Nanostructures for Electrical Energy Storage (NEES), an Energy Frontier Research Center funded by the U.S. Department of Energy, Office of Science, Office of Basic Energy Sciences under Award Number DESC0001160. K.G. is partially supported by the L-3 Communications fellowship.

Supporting Information Available: Further information discussing XPS experiments before and after lithiation of the MWCNT/RuO_2 core@shell heteronanostructure, as well as XRD patterns of the MWCNT/RuO_2. This material is available free of charge *via* the Internet at http://pubs.acs.org.

REFERENCES AND NOTES

1. Jung, Y. S.; Cavanagh, A. S.; Dillon, A. C.; Groner, M. D.; George, S. M.; Lee, S.-H. Enhanced Stability of $LiCoO_2$ Cathodes in Lithium-Ion Batteries Using Surface Modification by Atomic Layer Deposition. *J. Electrochem. Soc.* **2010**, *157*, A75–A81.
2. Jung, Y. S.; Cavanagh, A. S.; Riley, L. A.; Kang, S.-H.; Dillon, A. C.; Groner, M. D.; George, S. M.; Lee, S.-H. Ultrathin Direct Atomic Layer Deposition on Composite Electrodes for Highly Durable and Safe Li-Ion Batteries. *Adv. Mater.* **2010**, *22*, 2172.
3. Scott, I. D.; Jung, Y. S.; Cavanagh, A. S.; An, Y. F.; Dillon, A. C.; George, S. M.; Lee, S. H. Ultrathin Coatings on Nano-$LiCoO_2$ for Li-Ion Vehicular Applications. *Nano Lett.* **2011**, *11*, 414–418.
4. Cheng, H.-M.; Wang, F.-M.; Chu, J. P.; Santhanam, R.; Rick, J.; Lo, S.-C. Enhanced Cycleabity in Lithium Ion Batteries: Resulting From Atomic Layer Depostion of Al_2O_3 or TiO_2 on $LiCoO_2$ Electrodes. *J. Phys. Chem. C* **2012**, *116*, 7629–7637.
5. Lee, J.-T.; Wang, F.-M.; Cheng, C.-S.; Li, C.-C.; Lin, C.-H. Low-Temperature Atomic Layer Deposited Al_2O_3 Thin Film on Layer Structure Cathode for Enhanced Cycleability in Lithium-Ion Batteries. *Electrochim. Acta* **2010**, *55*, 4002–4006.
6. Jung, Y. S.; Cavanagh, A. S.; Yan, Y. F.; George, S. M.; Manthiram, A. Effects of Atomic Layer Deposition of Al_2O_3 on the $Li[Li_{0.20}Mn_{0.54}Ni_{0.13}Co_{0.13}]O$-2 Cathode for Lithium-Ion Batteries. *J. Electrochem. Soc.* **2011**, *158*, A1298–A1302.
7. Zhao, J. Q.; Wang, Y. Ultrathin Surface Coatings for Improved Electrochemical Performance of Lithium Ion Battery Electrodes at Elevated Temperature. *J. Phys. Chem. C* **2012**, *116*, 11867–11876.
8. Riley, L. A.; Cavanagh, A. S.; George, S. M.; Jung, Y. S.; Yan, Y.; Lee, S.-H.; Dillon, A. C. Conformal Surface Coatings to Enable High Volume Expansion Li-Ion Anode Materials. *ChemPhysChem* **2010**, *11*, 2124–2130.
9. He, Y.; Yu, X.; Wang, Y.; Li, H.; Huang, X. Alumina-Coated Patterned Amorphous Silicon as the Anode for a Lithium-Ion Battery with High Coulombic Efficiency. *Adv. Mater.* **2011**, *23*, 4938–4941.
10. Riley, L.; Cavanagh, A.; George, S.; Lee, S.; Dillon, A. Improved Mechanical Integrity of ALD-Coated Composite Electrodes for Li-Ion Batteries. *Electrochem. Solid State Lett.* **2011**, *14*, A29.
11. Lahiri, I.; Oh, S. M.; Hwang, J. Y.; Kang, C.; Choi, M.; Jeon, H.; Banerjee, R.; Sun, Y.-K.; Choi, W. Ultrathin Alumina-Coated Carbon Nanotubes as an Anode for High Capacity Li-Ion Batteries. *J. Mater. Chem.* **2011**, *21*, 13621–13626.
12. Rubloff, G. W.; Kozen, A. C.; Bok Lee, S. From Nanoscience to Solutions in Electrochemical Energy Storage. *J. Vac. Sci. Technol., A* **2013**, *31*, 1–21.
13. Knoops, H. C. M.; Donders, M. E.; Sanden, M. C. M. V. d.; Notten, P. H. L.; Kessels, W. M. M. Atomic Layer Deposition for Nanostructured Li-Ion Batteries. *J. Vac. Sci. Technol., A* **2012**, *30*, 010801.
14. Sundram, G. Atomic Layer Deposition for Energy Related Applications. AVS 60th International Symposium and Exhibition, Long Beach, CA, **Oct 27**–**Nov 1, 2013**; pp 1–39.
15. Kozen, A. C.; Pearse, A. J.; Lin, C. F.; Rubloff, G. W. Atomic Layer Deposition and *in-Situ* Characterization of Ultraclean Lithium Oxide and Lithium Hydroxide. *J. Phys. Chem. C* **2014**, *2014*, 27749–27753.
16. Cheah, S. K.; Perre, E.; Rooth, M.; Fondell, M.; Harsta, A.; Nyholm, L.; Boman, M.; Gustafsson, T.; Lu, J.; Simon, P.; *et al.* Self-Supported Three-Dimensional Nanoelectrodes for Microbattery Applications. *Nano Lett.* **2009**, *9*, 3230–3233.
17. Gerasopoulos, K.; Gerasopoulos, K.; Chen, X.; Chen, X.; Culver, J.; Culver, J.; Wang, C.; Wang, C.; Ghodssi, R. Self-Assembled Ni/TiO_2 Nanocomposite Anodes Synthesized *via* Electroless Plating and Atomic Layer Deposition on Biological Scaffolds. *Chem. Commun.* **2010**, *46*, 7349–7351.
18. Gerasopoulos, K.; McCarthy, M.; Banerjee, P.; Fan, X.; Culver, J. N.; Ghodssi, R. Biofabrication Methods for the Patterned Assembly and Synthesis of Viral Nanotemplates. *Nanotechnology* **2010**, *21*, 055304.
19. Wang, W.; Tian, M.; Abdulagatov, A.; George, S. M.; Lee, Y. C.; Yang, R. G. Three-Dimensional Ni/TiO_2 Nanowire Network for High Areal Capacity Lithium Ion Microbattery Applications. *Nano Lett.* **2012**, *12*, 655–660.
20. Donders, M. E.; Knoops, H. C. M.; Kessels, W. M. M.; Notten, P. H. L. Co_3O_4 as Anode Material for Thin Film Micro-Batteries Prepared by Remote Plasma Atomic Layer Deposition. *J. Power Sources* **2012**, *203*, 72–77.
21. Li, X. F.; Meng, X. B.; Liu, J.; Geng, D. S.; Zhang, Y.; Banis, M. N.; Li, Y. L.; Yang, J. L.; Li, R. Y.; Sun, X. L.; *et al.* Tin Oxide with Controlled Morphology and Crystallinity by Atomic Layer Deposition onto Graphene Nanosheets for Enhanced Lithium Storage. *Adv. Funct. Mater.* **2012**, *22*, 1647–1654.
22. Chen, X. Y.; Pomerantseva, E.; Banerjee, P.; Gregorczyk, K.; Ghodssi, R.; Rubloff, G. Ozone-Based Atomic Layer Deposition of Crystalline V_2O_5 Films for High Performance Electrochemical Energy Storage. *Chem. Mater.* **2012**, *24*, 1255–1261.
23. Gerasopoulos, K.; Pomerantseva, E.; McCarthy, M.; Brown, A.; Wang, C.; Culver, J.; Ghodssi, R. Hierarchical Three-Dimensional Microbattery Electrodes Combining Bottom-Up Self-Assembly and Top-Down Micromachining. *ACS Nano* **2012**, *6*, 6422–6432.
24. Pomerantseva, E.; Gerasopoulos, K.; Chen, X. Y.; Rubloff, G.; Ghodssi, R. Electrochemical Performance of the Nanostructured Biotemplated V_2O_5 Cathode for Lithium-Ion Batteries. *J. Power Sources* **2012**, *206*, 282–287.
25. Chen, X.; Zhu, H.; Chen, Y.-C.; Shang, Y.; Cao, A.; Hu, L.; Rubloff, G. W. MWCNT/V_2O_5 Core/Shell Sponge for High Areal Capacity and Power Density Li-Ion Cathodes. *ACS Nano* **2012**, *6*, 7948–7955.
26. Liu, C.; Gillette, E. I.; Chen, X.; Pearse, A. J.; Kozen, A. C.; Schroeder, M. A.; Gregorczyk, K. E.; Lee, S. B.; Rubloff, G. W. An All-in-One Nanopore Battery Array. *Nat. Nanotechnol.* **2014**, *9*, 1031–1039.
27. Cabana, J.; Monconduit, L.; Larcher, D.; Palacin, M. R. Beyond Intercalation-Based Li-Ion Batteries: the State of the Art and Challenges of Electrode Materials Reacting Through Conversion Reactions. *Adv. Mater.* **2010**, *22*, E170–E192.
28. Balaya, P.; Li, H.; Kienle, L.; Maier, J. Fully Reversible Homogeneous and Heterogeneous Li Storage in RuO_2 with High Capacity. *Adv. Funct. Mater.* **2003**, *13*, 621–625.
29. Delmer, O.; Balaya, P.; Kienle, L.; Maier, J. Enhanced Potential of Amorphous Electrode Materials: Case Study of RuO_2. *Adv. Mater.* **2008**, *20*, 501–505.
30. Gregorczyk, K.; Henn-Lecordier, L.; Gatineau, J.; Dussarrat, C.; Rubloff, G. Atomic Layer Deposition of Ruthenium Using the Novel Precursor Bis(2,6,6-Trimethyl-Cyclohexadienyl)Ruthenium. *Chem. Mater.* **2011**, *23*, 2650–2656.
31. Park, S. J.; Kim, W. H.; Maeng, W. J.; Yang, Y. S.; Park, C. G.; Kim, H.; Lee, K. N.; Jung, S. W.; Seong, W. K. Effect Oxygen Exposure on the Quality of Atomic Layer Deposition of Ruthenium From Bis(Cyclopentadienyl)Ruthenium and Oxygen. *Thin Solid Films* **2008**, *516*, 7345–7349.
32. Kwon, O. K.; Kim, J. H.; Park, H. S.; Kang, S. W. Atomic Layer Deposition of Ruthenium Thin Films for Copper Glue Layer. *J. Electrochem. Soc.* **2004**, *151*, G109–G112.
33. Kwon, S. H.; Kwon, O. K.; Kim, J. H.; Jeong, S. J.; Kim, S. W.; Kang, S. W. Improvement of the Morphological Stability by Stacking RuO_2 on Ru Thin Films with Atomic Layer Deposition. *J. Electrochem. Soc.* **2007**, *154*, H773–H777.
34. Kim, W. H.; Park, S. J.; Kim, D. Y.; Kim, H. Atomic Layer Deposition of Ruthenium and Ruthenium-Oxide Thin Films by Using a Ru(EtCp)(2) Precursor and Oxygen Gas. *J. Korean Phys. Soc.* **2009**, *55*, 32–37.
35. Salaun, A.; Trommer, J.; Newcomb, S. B.; Povey, I. M.; Salaun, M.; Keeney, L.; O'Mahony, A.; Pemble, M. E. Nucleation and Chemical Transformation of RuO_2 Films Grown on (100) Si Substrates by Atomic Layer Deposition. *Chem. Vap. Deposition* **2011**, *17*, 114–122.

36. Kim, J. H.; Kil, D. S.; Yeom, S. J.; Roh, J. S.; Kwak, N. J.; Kim, J. W. Modified Atomic Layer Deposition of RuO_2 Thin Films for Capacitor Electrodes. *Appl. Phys. Lett.* **2007**, *91*, 052908.
37. Park, S. K.; Kanjolia, R.; Anthis, J.; Odedra, R.; Boag, N.; Wielunski, L.; Chabal, Y. J. Atomic Layer Deposition of Ru/RuO_2 Thin Films Studied by *in Situ* Infrared Spectroscopy. *Chem. Mater.* **2010**, *22*, 4867–4878.
38. Husekova, K.; Dobrocka, E.; Rosova, A.; Soltys, J.; Satka, A.; Fillot, F.; Frohlich, K. Growth of RuO_2 Thin Films by Liquid Injection Atomic Layer Deposition. *Thin Solid Films* **2010**, *518*, 4701–4704.
39. Min, Y. S.; Bae, E. J.; Jeong, K. S.; Cho, Y. J.; Lee, J. H.; Choi, W. B.; Park, G. S. Ruthenium Oxide Nanotube Arrays Fabricated by Atomic Layer Deposition Using a Carbon Nanotube Template. *Adv. Mater.* **2003**, *15*, 1019.
40. Gillot, F.; Boyanov, S.; Dupont, L.; Doublet, M. L.; Morcrette, A.; Monconduit, L.; Tarascon, J.-M. Electrochemical Reactivity and Design of NiP_2 Negative Electrodes for Secondary Li-Lon Batteries. *Chem. Mater.* **2005**, *17*, 6327–6337.
41. Balaya, P.; Bhattacharyya, A. J.; Jamnik, J.; Zhukovskii, Y. F.; Kotomin, E. A.; Maier, J. Nano-Ionics in the Context of Lithium Batteries. *J. Power Sources* **2006**, *159*, 171–178.
42. Delmer, O.; Maier, J. On the Chemical Potential of a Component in a Metastable Phase-Application to Li-Storage in the RuO(2)-Li System. *Phys. Chem. Chem. Phys.* **2009**, *11*, 6424–6429.
43. Zhukovskii, Y. F.; Balaya, P.; Kotomin, E. A.; Maier, J. Evidence for Interfacial-Storage Anomaly in Nanocomposites for Lithium Batteries From First-Principles Simulations. *Phys. Rev. Lett.* **2006**, *96*, 058302.
44. Gregorczyk, K. E.; Liu, Y.; Sullivan, J. P.; Rubloff, G. W. *In Situ* Transmission Electron Microscopy Study of Electrochemical Lithiation and Delithiation Cycling of the Conversion Anode RuO_2. *ACS Nano* **2013**, *7*, 6354–6360.
45. Hu, Y.-Y.; Liu, Z.; Nam, K.-W.; Borkiewicz, O. J.; Cheng, J.; Hua, X.; Dunstan, M. T.; Yu, X.; Wiaderek, K. M.; Du, L.-S.; *et al.* Origin of Additional Capacities in Metal Oxide Lithium-Ion Battery Electrodes. *Nat. Mater.* **2013**, *12*, 1130–1136.
46. George, S. M. Atomic Layer Deposition: an Overview. *Chem. Rev.* **2010**, *110*, 111–131.
47. Aaltonen, T.; Rahtu, A.; Ritala, M.; Leskela, M. Reaction Mechanism Studies on Atomic Layer Deposition of Ruthenium and Platinum. *Electrochem. Solid State Lett.* **2003**, *6*, C130–C133.
48. Mar, S. Y.; Chen, C. S.; Huang, Y. S.; Tiong, K. K. Characterization of RuO_2 Thin-Films by Raman-Spectroscopy. *Appl. Surf. Sci.* **1995**, *90*, 497–504.
49. Deng, S.; Zhang, Y.; Brozena, A. H.; Mayes, M. L.; Banerjee, P.; Chiou, W.-A.; Rubloff, G. W.; Schatz, G. C.; Wang, Y. Confined Propagation of Covalent Chemical Reactions on Single-Walled Carbon Nanotubes. *Nat. Commun.* **2011**, *2*, 382–386.
50. Meng, X. B.; Ionescu, M.; Banis, M. N.; Zhong, Y.; Liu, H.; Zhang, Y.; Sun, S. H.; Li, R. Y.; Sun, X. L. Heterostructural Coaxial Nanotubes of CNT@Fe2O3 *via* Atomic Layer Deposition: Effects of Surface Functionalization and Nitrogen-Doping. *J. Nanopart. Res.* **2011**, *13*, 1207–1218.
51. Farmer, D. B.; Gordon, R. G. Atomic Layer Deposition on Suspended Single-Walled Carbon Nanotubes *via* Gas-Phase Noncovalent Functionalization. *Nano Lett.* **2006**, *6*, 699–703.
52. Arico, A. S.; Bruce, P.; Scrosati, B.; Tarascon, J.-M.; Van Schalkwijk, W. Nanostructured Materials for Advanced Energy Conversion and Storage Devices. *Nat. Mater.* **2005**, *4*, 366–377.
53. Notley, S. M.; Fogden, A. Applied Surface Science. *Appl. Surf. Sci.* **2013**, *285*, 220–225.
54. Hu, L. B.; Wu, H.; Gao, Y. F.; Cao, A. Y.; Li, H. B.; McDough, J.; Xie, X.; Zhou, M.; Cui, Y. Silicon-Carbon Nanotube Coaxial Sponge as Li-Ion Anodes with High Areal Capacity. *Adv. Energy Mater.* **2011**, *1*, 523–527.